Pt-Doped α-Fe_2O_3 Thin Films Active for Photoelectrochemical Water Splitting

Yong-Sheng Hu,[†] Alan Kleiman-Shwarsctein,[‡] Arnold J. Forman,[§] Daniel Hazen,[†] Jung-Nam Park,[†] and Eric W. McFarland*,[†]

Department of Chemical Engineering, Materials Department, and Chemistry & Biochemistry Department, University of California at Santa Barbara, Santa Barbara, California 93106-5080

Received January 15, 2008
Revised Manuscript Received April 16, 2008

A low cost method for solar-to-chemical energy conversion would have a wide range of potential applications.[1–6] Photoelectrochemical (PEC) processes make use of energetic holes and electrons (h^+/e^-) produced by photon absorption to perform oxidation/reduction reactions. The first demonstration of a PEC process for water electrolysis ("water splitting") was by Fujishima and Honda in 1972 using a titania photoanode illuminated with ultraviolet light.[1] Water was oxidized on the anodic titania, $2h^+ + H_2O \rightarrow 1/2O_2 + 2H^+$, and the protons reduced at the counter electrode $2e^- + 2H^+ \rightarrow H_2$. Subsequently, the creation of an economical solar based PEC process to produce hydrogen using sunlight has been the goal of many researchers.

Compared to other semiconductors, hematite (α-Fe_2O_3) has many potential advantages for hydrogen production in PEC devices.[5b–17] It is an n-type semiconductor that is stable in most electrolytes at pH > 3 and has a relatively narrow bandgap, 2−2.2 eV, sufficient to utilize approximately 40% of the incident sunlight. Furthermore, it is abundant, inexpensive, and environmentally benign. To date, several factors have limited the use of hematite in photocatalytic hydrogen production applications including poor conductivity and high electron−hole pair recombination rates. In addition, the energy of the conduction band edge relative to the redox level of H^+/H_2 is thought to hinder charge transfer for the reduction reaction.

Several groups have devised strategies to overcome these limitations by tailoring the hematite structure to allow more efficient transport and collection of photogenerated charge carriers.[11,16] The addition of surface electrocatalysts (e.g., Pt, Au, RuO_2) on iron oxide photoelectrodes has also been proposed to improve the PEC performance; however, the dependence on loading and preparation is not yet clearly understood.[14,17] Most work has been devoted to doping the iron oxide with heteroatoms as a means of improving performance.[5b,6,8,10,11,14,15]

A large number of dopant species have been introduced into Fe_2O_3 attempting to improve performance including Ca^{2+}, Mg^{2+}, Cu^{2+}, Zn^{2+}, Si^{4+}, Ge^{4+}, Ti^{4+}, Pt^{4+}, V^{5+}, and Nb^{5+}.[5,6,8,10,11,14,15] Significant variations in the electronic properties have been achieved, including, for example, decreases in resistivity of more than 3 orders of magnitude with 0.2% doping with Mg^{2+}.[5b] In some cases, heteroatom doping changes the microstructure of the thin films. For example, Si-doped Fe_2O_3 thin films prepared by chemical vapor deposition showed a preferred (001) orientation.[11] Si has been reported as the most effective dopant for enhancing the PEC performance;[11] Ti has been shown to improve the charge transport properties and the overall PEC performance.[5c] In samples prepared by spray pyrolysis, previous work has suggested that Pt doping decreased PEC performance in samples compared to undoped controls.[14]

In the past decade, a wide variety of Fe_2O_3 syntheses have been developed including sol−gel,[17,22] thermal oxidation,[8] chemical vapor deposition (CVD),[11] metal organic decomposition (MOD),[6] spray pyrolysis (SP),[13,14] and ultrasonic spray pyrolysis (USP).[11] The film morphologies have included nanostructures such as nanobelts, nanorods, and nanowires,[16,18,19] as well as mesoporous structures.[20,21] The synthesis of semiconductor electrodes by electrodeposition

* Corresponding author. E-mail: mcfar@engineering.ucsb.edu.
[†] Department of Chemical Engineering.
[‡] Materials Department.
[§] Chemistry & Biochemistry Department.

(1) (a) Fujishima, A.; Honda, K. *Nature* **1972**, *238*, 37. (b) Khaselev, O.; Turner, J. A. *Science* **1998**, *280*, 425. (c) Zou, Z. G.; Ye, J. H.; Sayama, K.; Arakawa, H. *Nature* **2001**, *414*, 625. (d) Gratzel, M. *Nature* **2001**, *414*, 338. (e) Maeda, K.; Teramura, K.; Lu, D. L.; Takata, T.; Saito, N.; Inoue, Y.; Domen, K. *Nature* **2006**, *440*, 295.
(2) Tryk, D. A.; Fujishima, A.; Honda, K. *Electrochim. Acta* **2000**, 2363.
(3) (a) Miller, E. L.; Rocheleau, R. E.; Khan, S. *Int. J. Hydrogen Energy* **2004**, *29*, 907. (b) Miller, E. L.; Paluselli, D.; Marsen, B.; Rocheleau, R. E. *Sol. Energy Mater. Sol. Cells* **2005**, *88*, 131.
(4) Bak, T.; Nowotny, J.; Rekas, M.; Sorrell, C. C. *Int. J. Hydrogen Energy* **2002**, *27*, 991.
(5) (a) Murphy, A. B.; Barnes, P. R. F.; Randeniya, L. K.; Plumb, I. C.; Grey, I. E.; Horne, M. D.; Glasscock, J. A. *Int. J. Hydrogen Energy* **2006**, *31*, 1999. (b) Mohanty, S.; Ghose, J. *J. Phys. Chem. Solids* **1992**, *53*, 81. (c) Glasscock, J. A.; Barnes, P. R. F.; Plumb, I. C.; Savvides, N. *J. Phys. Chem. C* **2007**, *111*, 16477.
(6) Arai, T.; Konishi, Y.; Iwasaki, Y.; Sugihara, H.; Sayama, K. *J. Comb. Chem.* **2007**, *9*, 574.
(7) (a) Hardee, K. L.; Bard, A. J. J. *Electrochem. Soc.* **1976**, *123*, 1024. (b) Leland, J. K.; Bard, A. J. *J. Phys. Chem.* **1987**, *91*, 5076.
(8) Shinar, R.; Kennedy, J. H. *Sol. Energy Mater.* **1982**, *6*, 323.
(9) Yeh, L. S. R.; Hackerman, N. *J. Electrochem. Soc.* **1977**, *124*, 833.
(10) (a) Leygraf, C.; Hendewerk, M.; Somorjai, G. A. *Proc. Natl. Acad. Sci. U.S.A.* **1982**, *79*, 5739. (b) Turner, J. E.; Hendewerk, M.; Parmeter, J.; Neiman, D.; Somorjai, G. A. *J. Electrochem. Soc.* **1984**, *131*, 1777. (c) Khader, M. M.; Vurens; G. H.; Kim, I. K.; Salmeron, M.; Somorjai, G. A. *J. Am. Chem. Soc.* **1987**, *109*, 3581.
(11) (a) Bjorksten, U.; Moser, J.; Gratzel, M. *Chem. Mater.* **1994**, *6*, 858. (b) Duret, A.; Gratzel, M. *J. Phys. Chem. B* **2005**, *109*, 17184. (c) Kay, A.; Cesar, I.; Gratzel, M. *J. Am. Chem. Soc.* **2006**, *128*, 15714.
(12) Dare-Edwards, M. P.; Goodenough, J. B.; Hamnett, A.; Trevellick, P. R. *J. Chem. Soc., Faraday Trans. 1* **1983**, *79*, 2027.
(13) Khan, S. U. M.; Akikusa, J. *J. Phys. Chem. B* **1999**, *103*, 7184.
(14) Sartoretti, C. J.; Alexander, B. D.; Solarska, R.; Rutkowska, I. A.; Augustynski, J.; Cerny, R. *J. Phys. Chem. B* **2005**, *109*, 13685.
(15) Aroutiounian, V. M.; Arakelyan, V. M.; Shahnazaryan, G. E.; Stepanyan, G. M.; Khachaturyan, E. A.; Wang, H.; Turner, J. A. *Sol. Energy* **2006**, *80*, 1098.
(16) (a) Beermann, N.; Vayssieres, L.; Lindquist, S. E.; Hagfeldt, A. *J. Electrochem. Soc.* **2000**, *147*, 2456. (b) Lindgren, T.; Wang, H. L.; Beermann, N.; Vayssieres, L.; Hagfeldt, A.; Lindquist, S. E. *Sol. Energy Mater. Sol. Cells* **2002**, *71*, 231.
(17) Watanabe, A.; Kozuka, H. *J. Phys. Chem. B* **2003**, *107*, 12713.
(18) (a) Fu, Y. Y.; Chen, J.; Zhang, H. *Chem. Phys. Lett.* **2001**, *350*, 491. (b) We, X. G.; Wang, S. H.; Ding, Y.; Wang, Z. L.; Yang, S. H. *J. Phys. Chem. B* **2005**, *109*, 215. (c) Fan, Z. Y.; Wen, X. G.; Yang, S. H.; Lu, J. G. *Appl. Phys. Lett.* **2005**, *87*, 013113.
(19) Wu, C. Z.; Yin, P.; Zhu, X.; Ou Yang, C. Z.; Xie, Y. *J. Phys. Chem. B* **2006**, *110*, 17806.
(20) Brezesinski, T.; Groenewolt, M.; Antonietti, M.; Smarsly, B. *Angew. Chem., Int. Ed.* **2006**, *45*, 781.
(21) Prakasam, H. E.; Varghese, O. K.; Paulose, M.; Mor, G. K.; Grimes, C. A. *Nanotechnology* **2006**, *17*, 4285.
(22) Zhong, L. S.; Hu, J. S.; Liang, H. P.; Cao, A. M.; Song, W. G.; Wan, L. J. *Adv. Mater.* **2006**, *18*, 2426.

10.1021/cm800144q CCC: $40.75
Published on Web 06/03/2008

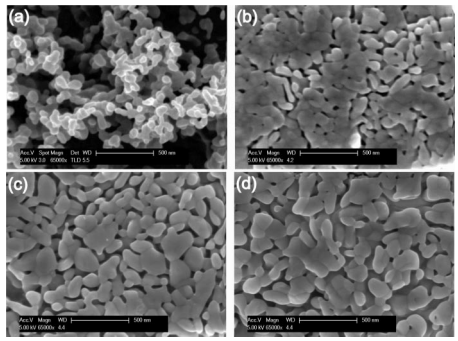

Figure 1. SEM of undoped and Pt-doped iron oxide thin films on Pt/Ti coated quartz: (a) 0% Pt, (b) 2% Pt, (c) 5% Pt, and (d) 10% Pt.

has many advantages including electrical contact, precise control of microstructure, and the potential for codepositing dopant elements.[23] Furthermore, large-scale superstructures and nanoscale microstructures can be created economically with electrodeposition.

There have been few reports on the synthesis of hematite films by electrodeposition[24] and no reports of electrodeposition of doped hematite. We report here an electrochemical route to prepare thin film photoanodes of nanocrystalline Pt-doped iron oxide which show improvement in PEC performance compared to pure iron oxide thin films prepared identically. Our work addresses the following questions: (a) Can Pt be introduced into α-Fe_2O_3 by coelectrodeposition? (b) Will the Pt be uniformly distributed or segregated? (c) Will the presence of Pt atoms as potential electron donors improve the PEC performance of photoanodes?

Following electrodeposition, the as-prepared thin films are yellowish in color and were identified as iron hydroxides by Raman spectroscopy. To obtain crystalline hematite films, samples were typically calcined at 700 °C for 4 h. Two thermally resistant and electronically conductive substrates were used: fluorine-doped tin oxide (FTO) on glass—stable to 600 °C, and Pt (1.5 μm)/Ti (0.5 μm) coated quartz—stable to 800 °C. In general, the samples calcined at 700 °C show the best performance.

Figure 1 compares the morphology of undoped and Pt-doped iron oxide thin films on Pt/Ti coated quartz. The change of the morphology before and after Pt-doping is striking. The Pt-doped films appear more uniform and dense than those of undoped controls (Note that the percentages of 2, 5, and 10% are referenced to the molar ratio of Pt/(Pt + Fe) in the electrolyte; the same convention is used in the following text and figures). Figure 2a and Figure S1 (Supporting Information) show the XRD patterns of the undoped and Pt-doped iron oxide thin films. With the exception of the marked substrate peaks, the XRD data is consistent with the rhombohedral symmetry of Fe_2O_3 (space group: $R3c$(167), $a = 0.5035$, $b = 0.5035$, $c = 1.3748$ nm; JCPDS card No. 33-0664) indicating the presence of a crystalline hematite phase and absence of other impurity

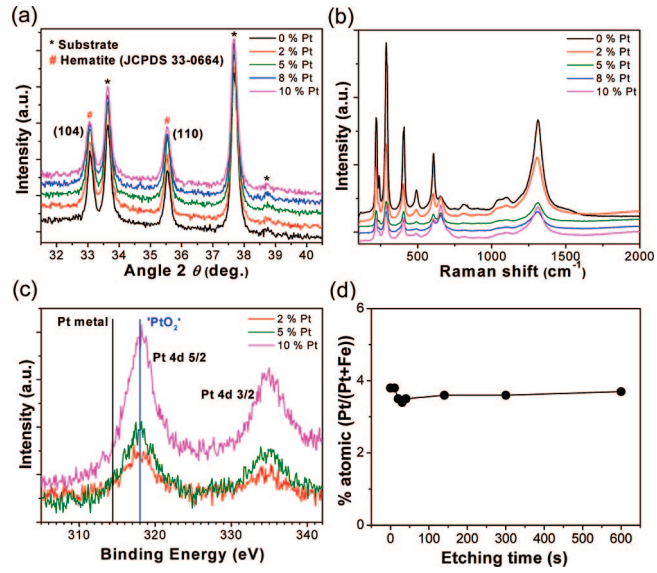

Figure 2. Characterizations of undoped and Pt-doped iron oxide thin films on FTO: (a) XRD patterns, (b) Raman spectra, (c) XPS spectra, and (d) XPS etching profile.

phases, including PtO_2 or Pt, at a level greater than the instrument sensitivity.

Raman spectra for both the undoped and Pt-doped iron oxide thin films, Figure 2b, show peaks ascribed to the α-Fe_2O_3 crystalline phase.[25] There is also a peak located at approximately 657 cm^{-1} which was previously assigned to magnetite (Fe_3O_4) or a disordered phase (possibly induced by the presence of FeO).[13,25] This peak increases in intensity with increasing Pt concentration whereas the 604 cm^{-1} peak decreases in intensity (see also Figure S2, Supporting Information). The intensity ratio (604 cm^{-1}/657 cm^{-1}) decreases from 3.4 to 0.3 with Pt increasing from 0% to 10%. XPS does not support the presence of a magnetite phase or FeO, Figure S3 (Supporting Information), since the Fe 2p spectra do not change before and after Pt doping. The change in the Raman spectra without a change in oxidation state (by XPS) suggests that there is a change in surface structure responsible for the variation. Further characterization, including extended X-ray absorption fine structure (EXAFS) and ^{57}Fe Mossbauer spectroscopy, would help to fully understand the changes. The Pt 4d spectra, Figure 2c, show only Pt^{4+} (no Pt^0) in the doped films. The XPS, together with the XRD and Raman observations, support the proposition that Pt was introduced into the lattice of the calcined α-Fe_2O_3 by coelectrodeposition. From the survey spectra of the Pt-doped iron oxide films, the Pt concentration on the surface can be approximated. The atomic percentages of Pt in films prepared from deposition solutions of 2, 5, and 10 atomic percent were approximately 2, 4, and 7%, respectively.

The distribution of Pt as a function of depth within the film was examined in the 5% Pt-doped sample by serial XPS measurements during controlled ion etching. Figure 2d presents the XPS etching profile obtained from the film before and after Ar^+ etching. A voltage of 4 kV and an ion beam current of 10 mA/cm^2 were used, resulting in an etching rate of approximately 20 nm/min. The etching time

(23) (a) Choi, K. S.; Lichtenegger, H. C.; Stucky, G. D.; McFarland, E. W. *J. Am. Chem. Soc.* **2002**, *124*, 12402. (b) Baeck, S. H.; Jaramillo, T.; Stucky, G. D.; McFarland, E. W. *Chem. Mater.* **2003**, *15*, 3411. (c) Jaramillo, T.; Baeck, S. H.; Kleiman-Shwarsctein, A.; Choi, K. S.; Stucky, G. D.; McFarland, E. W. *J. Comb. Chem.* **2005**, *7*, 264.

(24) Schrebler, R.; Bello, K.; Vera, F.; Cury, P.; Munoz, E.; deRio, R.; Meier, H. G.; Cordova, R.; Dalchiele, E. A. *Electrochem. Solid State Lett.* **2006**, *9*, C110.

(25) deFaria, D. L. A.; Silva, S. V.; deOliveira, M. T. *J. Raman Spectrosc.* **1997**, *28*, 873.

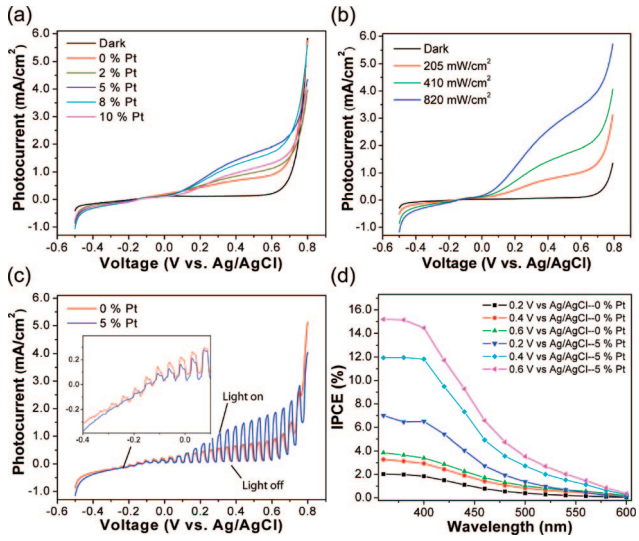

Figure 3. Photoelectrochemical performance of undoped and Pt-doped iron oxide thin films on Pt/Ti coated quartz: (a) $I-V$ curves of Pt-doped iron oxide thin films with different Pt concentrations under 410 mW/cm^2 illumination, (b) $I-V$ curves of 5% Pt-doped iron oxide with different light intensities, (c) chopped $I-V$ curves of undoped and 5% Pt-doped iron oxide thin films, and (d) IPCE performance of 5% Pt-doped and undoped iron oxide thin films at different applied potentials.

was varied from 0 to 10 min. The atomic ratio of Pt/(Pt + Fe) was observed to be constant (~4%), indicating that the surface and bulk have approximately the same Pt concentration.

Figure 3a shows the current−potential ($I-V$) curves of the undoped and Pt-doped iron oxide films in 1 M NaOH solution (pH = 13.6) in the dark and when illuminated. In the dark, the $I-V$ response for both samples is similar and shows no evidence of enhanced electrocatalytic activity due to the dopant. The photocurrent observed under illumination is a direct measure of the rate of water splitting and reflects the number of charge carriers produced from the incident light and their subsequent participation in water oxidation reaction on the photoanode and hydrogen ion reduction on the counter electrode.

The photocurrent for the undoped sample is slightly higher than that of Pt-doped samples at a low potential range of −0.10 to 0.10 V though it is rather low (<0.3 mA/cm^2) (see Figure S4, Supporting Information). However, the Pt-doped iron oxide thin films show a much higher photocurrent at a higher potential than that of undoped samples. Among all the compositions, the 5% Pt-doped sample exhibits the highest relative PEC performance. For example, at 0.4 V vs Ag/AgCl, the photocurrent density is 1.43 mA/cm^2 compared to the undoped sample, 0.69 mA/cm^2.

It can also be seen in Figure 3b that the photocurrent intensity increases with light intensity. Figure S5, Supporting Information, presents the relationship between photocurrent and light intensity for the undoped and 5% Pt-doped iron oxide thin films at different applied potentials. At these potentials, the photocurrent−light intensity relationship for the 5% Pt doped sample measured is approximately linear which suggests that saturation has not been reached and there is a relatively low rate of recombination. For the undoped sample there is a square-root relationship suggesting a relatively high recombination rate.[16] From the $I-V$ curves obtained by using a chopped white light source, Figure 3c, the photocurrent onset potential for the undoped sample is ~−0.3 V whereas the value is ~−0.2 V for the Pt-doped sample, which is consistent with what was observed in $I-V$ curves at a low potential region. This might result from the electronic structure change of α-Fe_2O_3 after Pt doping. The photocurrent obtained in the chopped $I-V$ curves is in good agreement with steady state $I-V$ curves, Figure 3a.

The incident photon-to-current efficiency (IPCE) as a function of wavelength for the undoped and 5% Pt-doped iron oxide thin films at different applied potentials is shown in Figure 3d. The IPCE of the Pt-doped sample is significantly greater under all conditions than that of the undoped sample (e.g., at 0.4 V, ~12% vs 3% (400 nm)). The UV−vis absorption spectra (not shown) qualitatively follow the observed IPCE behavior between 380 and 600 nm. The overall energy efficiency at different wavelengths and applied potentials can be calculated based on the light and electrical energy inputs, Efficiency = $[(1.23 - E_{appl}) \times i_{photocurrent}]/j_{photons}$. The best performing Pt-doped sample at 400 nm and 0.46 V (vs two-electrode system) would yield an overall energy efficiency of ~3%, which is nearly 4 times higher than that of the undoped sample.

Pt in hematite may act in several ways. First, Pt acts as an electron donor due to the substitution of Fe^{3+} by Pt^{4+} in the hematite lattice. The increased donor concentration in the n-type doping would translate into an improvement in the conductivity and enhance charge transfer while decreasing carrier recombination. Second, the increased donor concentration would increase the electric field across the space charge layer resulting in a higher charge separation efficiency. However, increasing the donor concentration would reduce the width of the space charge layer and the Pt^{4+} would have defect scattering/recombination properties that, at high concentrations, would negate the increased separation efficiency. The apparent optimum at 5% Pt doping may balance these competing effects most effectively and yield the best PEC performance. Third, the more compact doped films may have greater electrical interconnectivity which would facilitate charge transfer.

In conclusion, Pt was successfully introduced into α-Fe_2O_3 films by coelectrodeposition followed by high temperature calcination. The Pt was homogeneously distributed within the iron oxide film samples. The Pt-doped iron oxide films show an improvement in efficiency for photoelectrochemical water splitting compared to undoped samples consistent with the expected improvement in the electronic properties of the films after Pt-doping and in contrast to a previous report.[14] Further work on understanding the effect of Pt-doping into hematite on the mechanism and PEC behavior is ongoing.

Acknowledgment. Funding was provided by the DOE Hydrogen Program (DEFG36-05GO15040, -03GO13062), with partial support from the National Science Foundation (MRSEC-DMR05-20415). The work made use of the UCSB Nanofabrication Facility (NSF-funded NNIN). The authors thank Prof. Thomas F. Jaramillo, Wei Tang, Dr. Tom Mates, and Dr. Mark Cornish for advice and technical assistance.

Supporting Information Available: Additional information (PDF). This material is available free of charge via the Internet at http://www.pubs.acs.org.

CM800144Q